



This is a repository copy of *Modeling of inter-turn and inter-phase short-circuit of flux-switching permanent magnet motors*.

White Rose Research Online URL for this paper:
<http://eprints.whiterose.ac.uk/136563/>

Version: Accepted Version

Proceedings Paper:

Li, G. orcid.org/0000-0002-5956-4033, Zhu, Z.Q., Gabsi, M. et al. (2 more authors) (2018) Modeling of inter-turn and inter-phase short-circuit of flux-switching permanent magnet motors. In: 2018 IEEE Energy Conversion Congress and Exposition (ECCE). 2018 IEEE Energy Conversion Congress and Exposition (ECCE), 23-27 Sep 2018, Portland, USA. IEEE . ISBN 978-1-4799-7312-5

<https://doi.org/10.1109/ECCE.2018.8557351>

© 2018 IEEE. Personal use of this material is permitted. Permission from IEEE must be obtained for all other users, including reprinting/ republishing this material for advertising or promotional purposes, creating new collective works for resale or redistribution to servers or lists, or reuse of any copyrighted components of this work in other works. Reproduced in accordance with the publisher's self-archiving policy.

Reuse

Items deposited in White Rose Research Online are protected by copyright, with all rights reserved unless indicated otherwise. They may be downloaded and/or printed for private study, or other acts as permitted by national copyright laws. The publisher or other rights holders may allow further reproduction and re-use of the full text version. This is indicated by the licence information on the White Rose Research Online record for the item.

Takedown

If you consider content in White Rose Research Online to be in breach of UK law, please notify us by emailing eprints@whiterose.ac.uk including the URL of the record and the reason for the withdrawal request.



eprints@whiterose.ac.uk
<https://eprints.whiterose.ac.uk/>

Modeling of Inter-Turn and Inter-Phase Short-Circuit of Flux-Switching Permanent Magnet Motors

Guang-Jin Li, Senior Member, IEEE
Department of Electronic and Electric
Engineering
University of Sheffield
Sheffield, UK
g.li@sheffield.ac.uk
Antonio Griffo
Department of Electronic and Electric
Engineering
University of Sheffield
Sheffield, UK
a.griffo@sheffield.ac.uk

Zi-Qiang Zhu, Fellow, IEEE
Department of Electronic and Electric
Engineering
University of Sheffield
Sheffield, UK
z.q.zhu@sheffield.ac.uk
Javier Ojeda
Systèmes et applications des technologies de
l'information et de l'énergie (SATIE)
École normale supérieure Paris-Saclay
Cachan, France
javier.ojeda@satie.ens-cachan.fr

Mohamed Gabsi
Systèmes et applications des technologies de
l'information et de l'énergie (SATIE)
École normale supérieure Paris-Saclay
Cachan, France
Mohamed.GABSI@satie.ens-cachan.fr

Abstract— This paper presents an approach for detailed modelling of inter-turn and inter-phase short-circuit in a double layer, 12-slot and 10-pole Flux-Switching Permanent Magnet motor. This approach is based on MATLAB/Simulink and finite element analysis, and shows a fast and accurate estimation of the electromagnetic behavior for such machine under short-circuit conditions. Due to physical contact between different phase windings in the same stator slot, the inter-turn and inter-phase short-circuit in a double layer FSPM machine becomes a real possibility. However, this is rarely studied in the literature. Thus, this work contributes for the fault analysis of inter-turn and inter-phase short-circuit problems. Experimental tests have been carried out to validate the simulations.

Index Terms— fault diagnosis, flux-switching, inter-turn short circuit, permanent magnet, synchronous motor.

I. INTRODUCTION

FLUX-Switching Permanent Magnet (FSPM) motors have attracted increasing interest in the last two decades [1] [2] [3]. The common topology of the FSPM machines is given in Fig. 1, which shows that the polarities of each two adjacent permanent magnets are opposite. As a result, a flux focusing effect can be achieved, leading to high torque/power density. This is similar to that of a flux concentrating PM machine while with the permanent magnets mounted on the stator instead of on the rotor [4]. Since the phase flux linkages are bipolar [5], its torque density can be higher than other stator mounted permanent magnet machines with unipolar phase flux linkages such as the doubly salient permanent magnet machines [6]. In addition, since the PMs of a FSPM machine are protected by both U-shape sections of the stator teeth (Fig. 1), in case of flux weakening operation or short-circuit (SC), the risk of irreversible demagnetization of PMs in the FSPM machine is considerably lower compared to other PM motors. As a result, the FSPM machine is well suitable for applications requiring significant flux weakening capability such as constant power operation over a wide speed range. Furthermore, the rotor of a FSPM is similar to that of a switched reluctance motor, which makes the structure of a FSPM machine very simple and robust, and hence suitable for high speed applications [7].

In electrical machines, one of the most frequent faults is the inter-turn SC, which affects not only machine electromagnetic but also thermal and mechanical performances [8] - [9]. The severity of inter-turn SC could be the most critical [10]. It may lead to a local overheating in the stator windings, and hence resulting in the SC of the entire phase. It should be noted that the SC current produces demagnetizing magnetic field, which is similar to negative d-axis current (I_d) [11]. As a result this could lead to partial irreversible demagnetization and the phase no-load flux linkages might decline [12]. In order to maintain the output torque, the most direct way is to increase phase currents [13]. However, this will increase the copper loss. As a main heat source of electrical machines, the temperature increase due to copper losses could exceed the maximum allowable temperature of winding insulation materials. As a result, the SC can have destructive effect on electrical machines. Therefore, it is important to predict the influence of the inter-turn SC in or between phases.

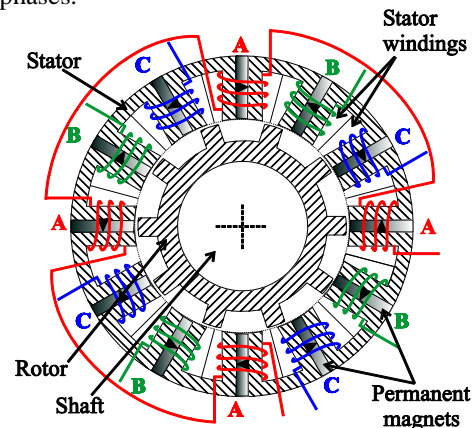


Fig. 1 Cross-sectional view of a FSPM 12-slot/10-pole. 4 coils of one phase are connected in series.

Numerous diagnosis methods for SC faults have been proposed in the literature, and a summary of different methods are given in [10]. In this paper, stator current monitoring method is employed to detect the inter-turn SC. This method is often considered as the most useful because it is nonintrusive and does not require extra equipment [14]. The inter-turn SC in

one phase of electrical machines are very widely studied in the literature. However, the inter-turn and inter-phase SC problems are rarely investigated. Thus, in order to fill in this gap, detailed analyses of such fault in a double layer FSPM have been carried out in this paper.

II. MODELING OF INTER-TURN SC IN TWO PHASES

A. Equivalent Circuit and Control Diagram

In order to compare and also to simplify the introduction of modelling methodologies of short-circuit in FSPM machines, a fault model of inter-turn SC in two independent phases of a FSPM 12-slot/10-pole is described. Then the obtained results will be compared against the inter-turn and inter-phase SC in section III. It is also worth noting that the inter-turn and inter-phase SC is more likely to happen in the machines with double layer windings while the inter-turn SC in two independent phases should be regarded as a rare event in electrical machines.

The winding configuration and the equivalent electric circuit of the investigated FSPM machine are shown in Fig. 2. As an example, the inter-turn SC in phases A and B are chosen. In Fig. 2 (b), i_A is the current in healthy windings, i_{SC1} is the SC current in faulty windings, while i_{total1} is the difference between the two previous currents. These definitions are also applicable for the phase B.

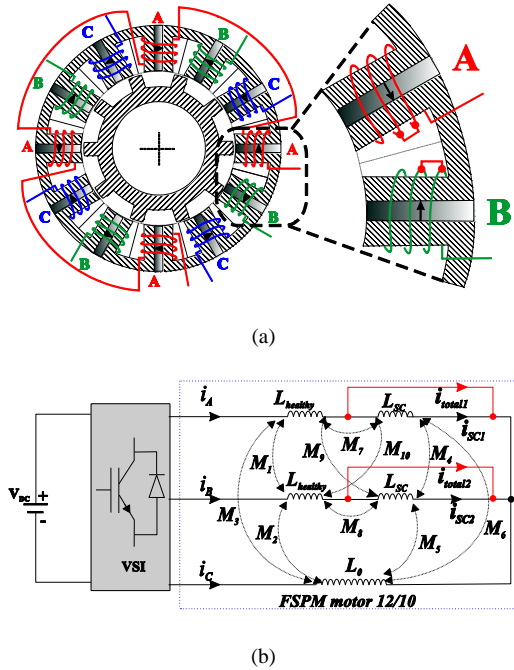


Fig. 2 Inter-turn SC in two independent phases of FSPM 12/10. (a) winding configuration, (b) equivalent electric circuit.

In Fig. 2 (b), L_0 , $L_{healthy}$ and L_{SC} are the total phase self-inductance, the self-inductances of the healthy and the short-circuited windings, respectively. M_1 is the mutual-inductance between the healthy windings of the phases A and B, M_2 and M_3 are the mutual-inductances between the healthy windings of phases A or B and the phase C, M_4 is the mutual-inductance between the short-circuited windings of the phases A and B, M_5 and M_6 are the mutual-inductances between the short-

circuited windings of the phases A or B and the phase C, M_7 and M_8 are the mutual-inductances between the healthy and short-circuited windings of the phases A and B while M_9 and M_{10} are the mutual-inductances between the healthy windings of the phases A or B and short-circuited windings of the phases B or A.

B. Electromagnetic and Mechanical Models

The electromagnetic model of one phase can be written as

$$v = R_0 i + L \frac{di}{dt} + e_0 \quad (1)$$

with

$$e_0 = \frac{d\Phi_f}{dt} = p\Omega \frac{d\Phi_f}{d\theta_e} \quad (2)$$

where v , i , R_0 , L and e_0 are the phase terminal voltage, the phase current, the resistance, the inductance and the back-EMF, respectively. Φ_f , p , Ω and θ_e are the no-load flux linkage calculated by 2D finite element method (FEM), the rotor pole number (for FSPM machines, p is equal to the pole pair number), the mechanical rotor speed and the electrical rotor angle, respectively. Assuming that the machine is supplied with sinewave currents, (1) can then be converted to matrix form as follows

$$[v] = [R][i] + p\Omega[L] \frac{d[i]}{d\theta_e} + p\Omega \frac{d[\Phi_f]}{d\theta_e} \quad (3)$$

where $[R]$, $[L]$, $[i]$ and $[\Phi_f]$ are the matrices of resistances, inductances (self and mutual), currents and no-load flux linkages, respectively. The phase resistance is measured directly by using the machine shown in Fig. 4 while $[L]$ and $[\Phi_f]$ are calculated by 2D FEM.

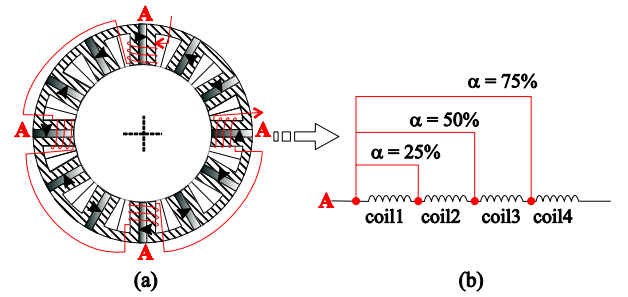


Fig. 3 Demonstration of inter-turn SC in one phase. (a) winding configuration of the phase A, (b) different numbers of turns short-circuited.

The details about winding configuration and the calculation of different SC percentages (α) - the number of short-circuited turns (n) over the total number of turns per phase (N) are shown in Fig. 3. By way of example, only the phase A is shown. In this paper, the windings are concentrated ones and each tooth is wound by one coil [Fig. 3 (a)]. This means that there are two coils located in each stator slot, leading to double layer winding configurations. In addition, all the coils of the same phase are connected in series. Since each phase is formed by 4 series connected coils, if one coil is short-circuited, α is equal to 25%, as can be seen in Fig. 3 (b).

Based on Fig. 2 and Fig. 3 and for simplicity, the percentages of SC turn numbers in phases A and B are

assumed to be equal, meaning $\alpha = \beta$, where β is the percentage of SC turn number of phase B and its definition is the same as α . Thus the percentages of healthy turn numbers are $1 - \alpha = 1 - \beta$. Generally, for a machine with one coil per phase, the self-inductance is proportional to the square of number of turns. Thus, the healthy ($L_{healthy}$) and faulty (L_{SC}) self-inductances of phases A and B can be calculated by

$$L_{healthy} = (1 - \alpha)^2 L_0 \text{ and } L_{SC} = \alpha^2 L_0 \quad (4)$$

However, the 2D FEM studies have shown that the magnetic coupling between coils of the same phase is significantly low. As a result, (4) is no longer valid. To calculate $L_{healthy}$ and L_{SC} of a phase formed by several coils, B. Vaseghi et al [15] have proposed a new method, which achieves satisfactory accuracy. Although the winding configuration used in [15] is distributed, the method can still be applied in the concentrated winding configuration.

By way of example, neglecting the mutual inductances between coils of the same phase and when $\alpha = 25\%$, the healthy and SC self-inductances can be calculated by [15]

$$\begin{cases} L_{healthy} = [3 + (1 - \alpha_{bob})^2] L_{bob} \\ L_{SC} = \alpha_{bob}^2 L_{bob} \end{cases} \quad (5)$$

where α_{bob} is the percentage of number of short-circuited turns over the total number of turns of one coil ($\alpha_{bob} = 4\alpha$), L_{bob} is the self-inductance of one coil ($L_0 \approx 4L_{bob}$). This has been verified by 2D FEM. It is found that the inductance of one coil is approximately one fourth of the phase inductance. Based on the same theory, the mutual-inductances can also be calculated as follows

$$\begin{cases} M_1 = (1 - \alpha)(1 - \beta)M_0 \\ M_2 = M_3 = (1 - \alpha)M_0 \\ M_4 = \alpha\beta M_0 \\ M_5 = M_6 = \alpha M_0 \\ M_7 = M_8 = \alpha_{bob}(1 - \alpha_{bob})L_{bob} = 0 \\ M_9 = M_{10} = (1 - \alpha)\beta M_0 \end{cases} \quad (6)$$

where M_0 is mutual-inductance between phases without SC. When $\alpha = 50\%$ and $\alpha = 75\%$, the healthy and SC self-inductances can be calculated by

$$\begin{cases} L_{healthy} = [(4 - q) + (1 - \alpha_{bob})^2] L_{bob} \\ L_{SC} = [(q - 1) + \alpha_{bob}^2] L_{bob} \end{cases} \quad (7)$$

where q is the SC coil number (integer value), which can change from 1 to 4 for $\alpha \geq 25\%$. The mutual-inductances can also be calculated using (6). With the previously obtained self- and mutual-inductances, the matrix of inductances in (3) is established as in (8).

$$[L] = \begin{bmatrix} L_{healthy} & M_1 & M_3 & M_7 & M_9 \\ M_1 & L_{healthy} & M_2 & M_{10} & M_8 \\ M_3 & M_2 & L_0 & M_6 & M_5 \\ M_7 & M_{10} & M_6 & L_{SC} & M_4 \\ M_9 & M_8 & M_5 & M_4 & L_{SC} \\ \underbrace{A \text{ healthy}} & \underbrace{B \text{ healthy}} & \underbrace{C} & \underbrace{A \text{ SC}} & \underbrace{B \text{ SC}} \end{bmatrix} \quad (8)$$

The resistances and the no-load flux linkages are directly proportional to the number of turns and much easier to calculate, thus not shown here to save space. Knowing that the

voltages of the SC windings are null, thus the matrix of voltages in (3) can be replaced by (9).

$$[v] = V_{max} \begin{bmatrix} \cos(p\theta + \pi/2 + \delta) \\ \cos(p\theta + 2\pi/3 + \pi/2 + \delta) \\ \cos(p\theta - 2\pi/3 + \pi/2 + \delta) \\ 0 \\ 0 \end{bmatrix} \quad (9)$$

Finally, the general mechanical model of the FSPM machine is the same as other types of electrical machines and can be described by (10).

$$C_{em} = p \frac{d[\Phi_f]^t}{d\theta_e} [i] = J \frac{d\Omega}{dt} + f\Omega + C_r \quad (10)$$

where C_{em} , J , f and C_r are the electromagnetic torque, the moment of inertial, the friction coefficient and the load torque, respectively.

C. Simulated and Experimental Results

The previously established electromagnetic and mechanical models are implemented in MATLAB/Simulink. In order to validate the simulated results, a FSPM machine (parameters are given in Table 1) shown in Fig. 4 is used for experimental tests. The control diagram shown in Fig. 5 is applied to drive this machine. This can be realized by using the dSPACE based programs, and a DC generator is used to provide load torque C_r . The three phases of the machine are supplied via a Voltage Source Inverter (VSI). The speed and the current are controlled by a PI controller and a hysteresis controller, respectively, as depicted in Fig. 5.

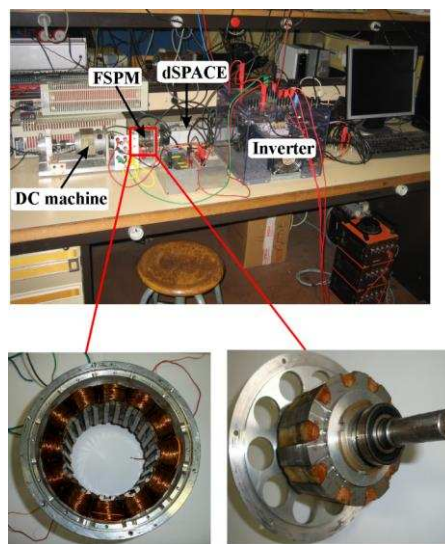


Fig. 4 Prototype of a FSPM 12/10 for experimental tests.

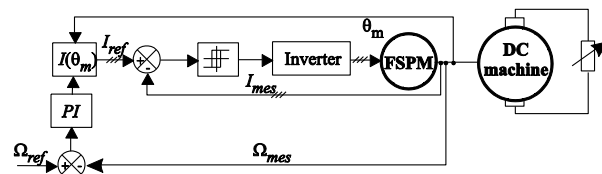
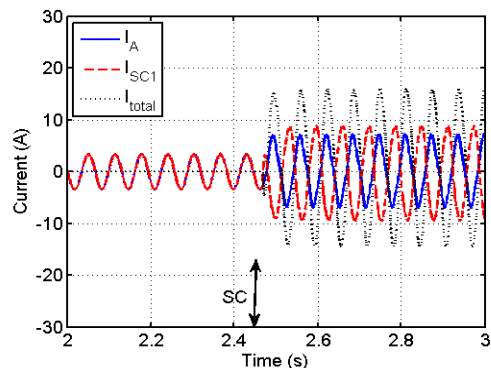
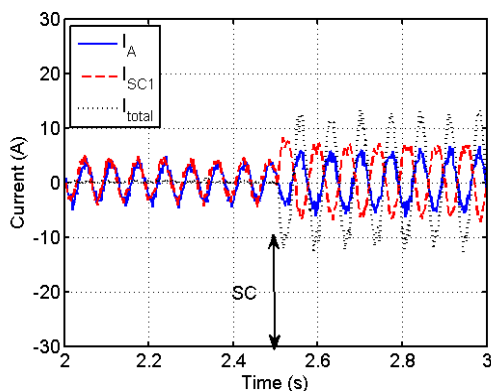


Fig. 5 Simplified diagram of a closed-loop FSPM drive. Ω_{ref} : reference speed, Ω_{mes} : measured speed, I_{ref} : reference current, I_{mes} : measured current, θ_m : rotor mechanical position.

A load torque (C_r) of 6 Nm and a reference speed (Ω_{ref}) of 10 rad/s are set for both simulation and experiment conditions. It is assumed that the FSPM operates under healthy mode till 2.4 seconds. Then, two inter-turn SCs happened simultaneously in phases A and B. In order to simplify the experimental tests, the percentages of SC turn numbers are set to $\alpha = \beta = 25\%$ (one coil is short-circuited). The inter-turn SC is depicted in Fig. 3 (only the phase A is presented, the SC in the phase B is the same as that in the phase A). In order to realize the inter-turn SC with different SC levels, each coil has two terminals and the 4 coils are connected in series outside the FSPM machine. Based on this configuration, the inter-turn SC can be artificially realized by short-circuiting the two terminals of coils [see Fig. 3 (b)] and α can change from 25% to 75% of one phase by a step of 25%.



(a)



(b)

Fig. 6 Simulated and measured currents for inter-turn SC in two phases. In this case, $\alpha = 25\%$. (a) simulated currents, (b) measured currents.

The simulated and measured currents and rotor speed, before and after the inter-turn SC in two phases, are shown in Fig. 6 and Fig. 7. Here, only $\alpha = \beta = 25\%$ is given and the results for other $\alpha = \beta$ have not been presented due to lack of space. The SC current (I_{SC2}) in the phase B has the same amplitude as I_{SC1} while with a phase shift angle of $2\pi/3$. Thus only the currents in the phase A are given and analyzed in this paper. After the SC, it is found that, regardless of the number of short-circuited turns, I_{total1} and I_A are always in phase while I_{SC1} and I_A are always opposite. Moreover, at low rotor speed ($\Omega = 10$ rad/s), I_{total1} and I_A increase considerably while the

variation of I_{SC1} versus α is very low as can be calculated by (11). For simplicity, the mutual inductances are neglected in this equation, because they are relatively low in comparison with the self-inductance and phase resistance.

$$I_{SC1} \approx \frac{|\alpha E_{max}|}{\sqrt{(\alpha R_0)^2 + (\alpha^2 \omega L_0)^2}} = \frac{|\omega \Phi_{fmax}|}{\sqrt{(R_0)^2 + (\alpha \omega L_0)^2}} \quad (11)$$

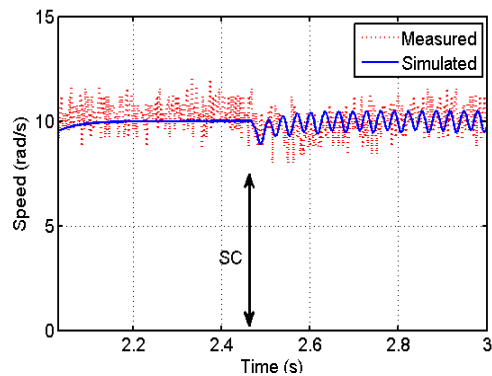


Fig. 7 Simulated and measured speed before and after the inter-turn SC in two independent phases for $\alpha = 25\%$.

III. MODELING OF INTER-TURN AND INTER-PHASE SC OF A FSPM

Compared to the distributed overlapping windings, the double layer concentrated and non-overlapping winding structure can have much shorter end-windings. Thus, for the same phase current, the machine with double layer concentrated windings generates significantly less copper losses, and hence lower temperature rise. This feature is important for some safety-critical applications such as more electrical aircraft, which has high operating temperatures. In these applications, any minimization of copper losses is desirable to minimize the maximum temperature. However, the main drawback of double layer structure is the physical contact between two layers in the same stator slots. In case of insulation material failure in stator slots, the conductors of different phases could be connected and the inter-turn and inter-phase SC forms accordingly. In order to study such fault on the electromagnetic behaviours of a 12-slot/10-pole FSPM machine, a MATLAB/Simulink based faulty model has been developed. The details are discussed in the following sections.

A. Equivalent Circuit and Electromagnetic Model

The inter-turn and inter-phase SC winding configuration, the equivalent electric circuit and the different levels of SC turn numbers α are shown in Fig. 8. Here, all the resistances and inductances are identical to those shown in Fig. 2. Nonetheless, the main difference is that the SC winding voltage (v_{SC}) is no longer null. On the contrary, it depends on the resistances, the inductances (self and mutual), the back-EMF and the SC currents as well as the rotor speed and can be calculated by (14). This expression establishes the relationship between the voltages (healthy and faulty) and the currents (healthy and faulty) and makes the analytical simulation possible.

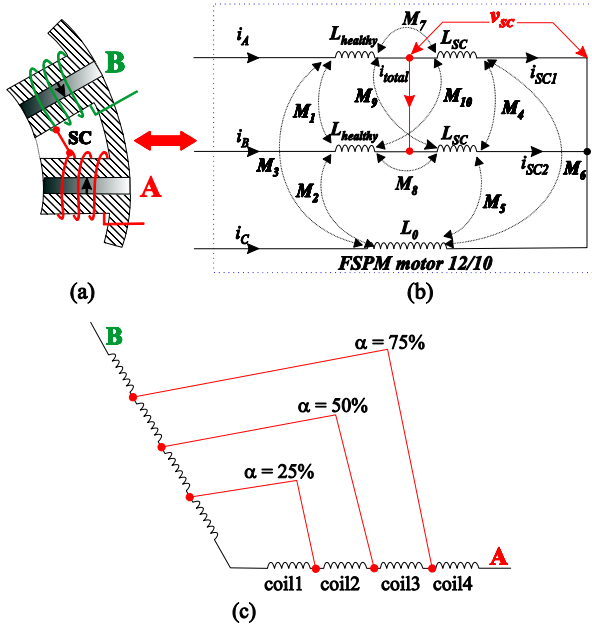


Fig. 8 (a) winding configuration, (b) equivalent circuit of the inter-turn and inter-phase SC, (c) different α of the 12-slot/10-pole FSPM machine.

Assuming that the three phase voltages (v_A , v_B and v_C) are known variables, thus (14) consists of five equations while with six unknown variables (five currents: i_A , i_B , i_C , i_{SC1} and

$$\begin{cases} v_A = L_{healthy} \frac{di_A}{dt} + (1 - \alpha)(R_0 i_A + e_A) + M_7 \frac{di_{SC1}}{dt} + M_1 \frac{di_B}{dt} + M_3 \frac{di_C}{dt} + M_9 \frac{di_{SC2}}{dt} + v_{SC} \\ v_B = L_{healthy} \frac{di_B}{dt} + (1 - \beta)(R_0 i_B + e_B) + M_1 \frac{di_A}{dt} + M_2 \frac{di_C}{dt} + M_8 \frac{di_{SC2}}{dt} + M_{10} \frac{di_{SC1}}{dt} + v_{SC} \\ v_C = L_0 \frac{di_C}{dt} + R_0 i_C + e_C + M_2 \frac{di_B}{dt} + M_3 \frac{di_A}{dt} + M_5 \frac{di_{SC2}}{dt} + M_6 \frac{di_{SC1}}{dt} \\ v_{SC} = L_{SC} \frac{di_{SC1}}{dt} + \alpha(R_0 i_{SC1} + e_A) + M_7 \frac{di_A}{dt} + M_{10} \frac{di_B}{dt} + M_6 \frac{di_C}{dt} + M_4 \frac{di_{SC2}}{dt} \\ v_{SC} = L_{SC} \frac{di_{SC2}}{dt} + \beta(R_0 i_{SC2} + e_B) + M_9 \frac{di_A}{dt} + M_8 \frac{di_B}{dt} + M_5 \frac{di_C}{dt} + M_4 \frac{di_{SC1}}{dt} \end{cases} \quad (14)$$

Relationship between the healthy and SC currents obtained based on Kirchoff's voltage law:

$$\begin{aligned} 0 = L_{SC} \frac{di_{SC1}}{dt} + \alpha(R_0 i_{SC1} + e_A) + M_7 \frac{di_A}{dt} + M_{10} \frac{di_B}{dt} + M_6 \frac{di_C}{dt} + M_4 \frac{di_{SC2}}{dt} - \\ \left[L_{SC} \frac{di_{SC2}}{dt} + \beta(R_0 i_{SC2} + e_B) + M_9 \frac{di_A}{dt} + M_8 \frac{di_B}{dt} + M_5 \frac{di_C}{dt} + M_4 \frac{di_{SC1}}{dt} \right] \end{aligned} \quad (15)$$

Final relationship between the voltages and the healthy and SC currents in case of inter-turn and inter-phase SC is:

$$\begin{bmatrix} v_A \\ v_B \\ v_C \\ 0 \\ 0 \end{bmatrix} = \begin{bmatrix} (1 - \alpha)R_0 & 0 & 0 & \alpha R_0 & 0 \\ 0 & (1 - \beta)R_0 & 0 & 0 & \beta R_0 \\ 0 & 0 & R_0 & 0 & 0 \\ 0 & 0 & 0 & \alpha R_0 & -\beta R_0 \\ -1 & -1 & 0 & 1 & 1 \end{bmatrix} \begin{bmatrix} i_A \\ i_B \\ i_C \\ i_{SC1} \\ i_{SC2} \end{bmatrix} + \begin{bmatrix} e_A \\ e_B \\ e_C \\ \alpha e_A - \beta e_B \\ 0 \end{bmatrix} + \begin{bmatrix} L_{healthy} + M_7 & M_1 + M_{10} & M_3 + M_6 & L_{SC} + M_7 & M_4 + M_9 \\ M_1 + M_9 & L_{healthy} + M_8 & M_2 + M_5 & M_4 + M_{10} & L_{SC} + M_8 \\ M_3 & M_2 & L_0 & M_6 & M_5 \\ M_7 - M_9 & M_{10} - M_8 & M_6 - M_5 & L_{SC} - M_4 & M_4 - L_{SC} \\ -1 & -1 & 0 & 1 & 1 \end{bmatrix} \frac{d}{dt} \begin{bmatrix} i_A \\ i_B \\ i_C \\ i_{SC1} \\ i_{SC2} \end{bmatrix} \quad (16)$$

i_{SC2} , one voltage: v_{SC}). In order to solve these equations, it is necessary to add another equation or to eliminate one unknown variable. The former could be realized by Kirchoff's current law. It allows to establish the relationship between currents in healthy windings and those in SC windings of the phases A and B, such as

$$0 = -i_A - i_B + i_{SC1} + i_{SC2} = -\frac{di_A}{dt} - \frac{di_B}{dt} + \frac{di_{SC1}}{dt} + \frac{di_{SC2}}{dt} \quad (12)$$

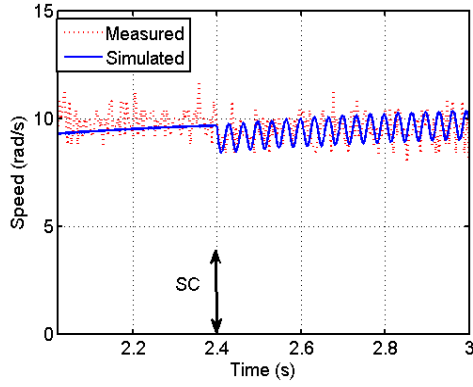
Then, based on Kirchoff's voltage law, v_{SC} can be eliminated by summing all the voltages of the closed-loop including the inter-turn and inter-phase SC windings [see (15)]. Finally, with the three equations obtained previously [see (12), (14) and (15)], a system with five equations and five unknown variables can be achieved, the matrix form of which is given in (16). After solving (16), the healthy and SC currents can be obtained. Knowing the back-EMFs of the healthy and faulty windings, the electromagnetic torque under faulty mode can then be calculated by (13).

$$C = \frac{(1 - \alpha)e_A i_A + (1 - \beta)e_B i_B + e_C i_C + \alpha e_A i_{SC1} + \beta e_B i_{SC2}}{\Omega} \quad (13)$$

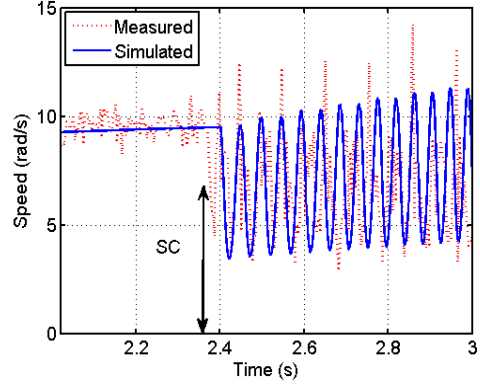
B. Simulated and Experimental Results

Similar to the studies in section II, simulations based on MATLAB/Simulink and experimental validations (see Fig. 4) for the inter-turn and inter-phase SC have been carried out as well. The simulated and measured results in terms of rotor speed and healthy as well as SC currents are shown in Fig. 9 and Fig. 10. Similar phenomena to the inter-turn SC in two phases have been observed. The speed drops and the speed

ripple increases considerably with the increase in α (see Fig. 9). The healthy current in the phase A increases significantly after the SC, which is almost five times higher than its value before the SC [see Fig. 10 (b) and Fig. 11 (b)]. This increase in healthy current is mainly because the speed controller tries to compensate the loss of healthy turns and the increase in braking torque generated by the short-circuited turns.

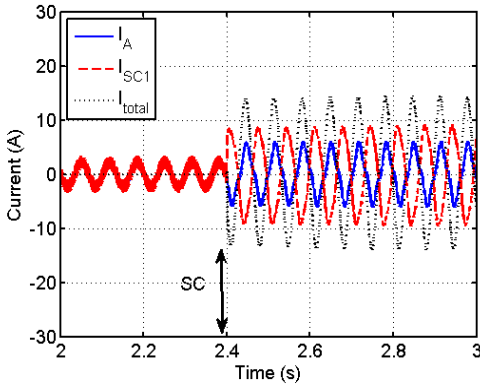


(a)

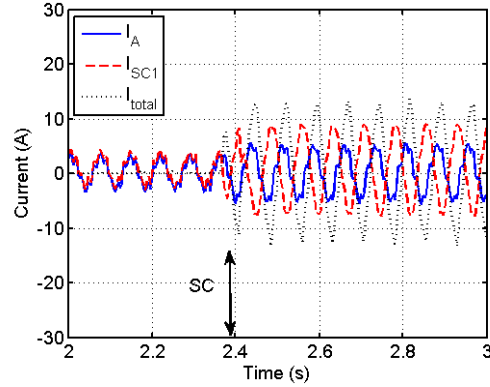


(b)

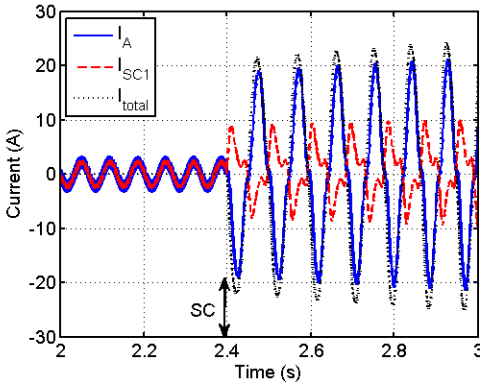
Fig. 9 Simulated and measured speeds before and after the inter-turn and inter-phase SC for different percentages of SC turns. (a) $\alpha = \beta = 25\%$, (b) $\alpha = \beta = 75\%$.



(a)

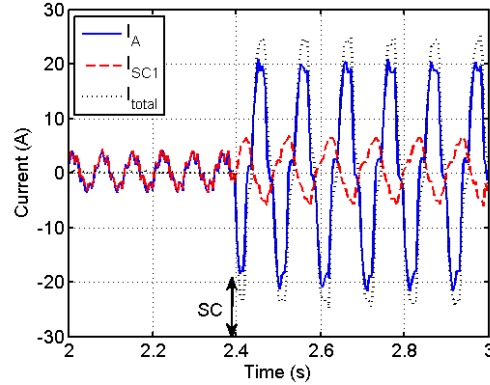


(a)



(b)

Fig. 10 Simulated currents for different levels of SC turn numbers in case of inter-turn and inter-phase SC. (a) $\alpha = \beta = 25\%$, (b) $\alpha = \beta = 75\%$.



(b)

Fig. 11 Measured currents for different levels of SC turn numbers in case of inter-turn and inter-phase SC. (a) $\alpha = \beta = 25\%$, (b) $\alpha = \beta = 75\%$.

It can be observed that the measured results match relatively well with the simulated ones. The discrepancy is mainly due to the fact that the end-winding has not been taken into account during the 2D FE calculations for the phase inductances.

It is well established that, at low rotor speed, the resistive influence due to phase resistances is dominant compared to the inductive influence due to phase inductances. Thus, in order to verify the model given in (16), the simulations and experimental tests at high rotor speed have also been performed. For both simulation and experimental conditions, the rotor speed and load torque are set to be 102 rad/s and 6 Nm, respectively. By way of example, the percentage of inter-turn SC turn number $\alpha = \beta = 25\%$ is chosen. The simulated and measured results are shown in Fig. 12 and Fig. 13. Again, a good agreement can be observed. This could finally validate the proposed inter-turn and inter-phase SC model.

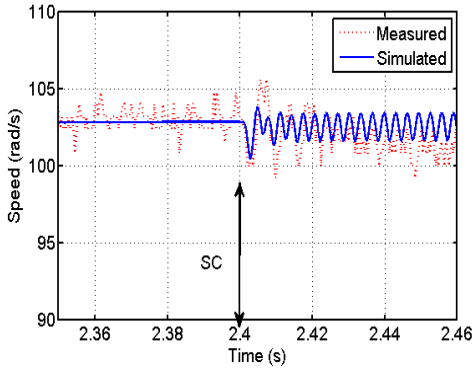
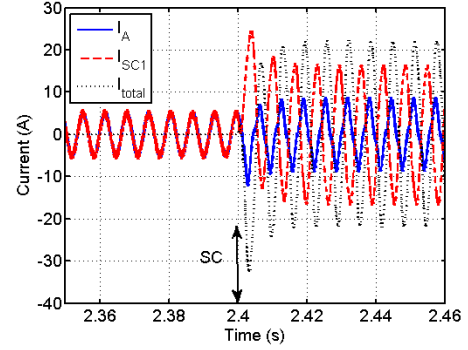


Fig. 12 Simulated and measured speed before and after the inter-turn and inter-phase SC for $\alpha = \beta = 25\%$ and at 102 rad/s.

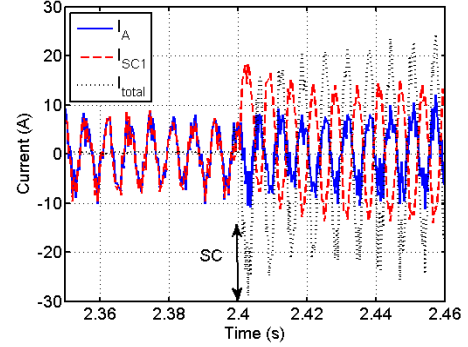
In comparison with the results for the rotor speed of 10 rad/s and $\alpha = \beta = 25\%$, after the SC at 102 rad/s, the speed drops and speed ripple changes slightly. This is the same case for the healthy current (I_A). However, the SC current increases considerably (from 9 A to 17A). The high SC currents together with the increase in the healthy currents will increase considerably the power losses. This could lead to an overheating of electrical machines under faulty mode. Thus, it is essential to predict the variation of SC currents for fault tolerant applications. Otherwise, a well-designed machine under healthy conditions could not satisfy the machine specifications under faulty conditions.

Comparing to the inter-turn SC in two independent phases, with the same percentage of SC turn number ($\alpha = \beta = 25\%$), the drop of rotor speed in the case of inter-turn and inter-phase SC is similar while its speed ripple is much higher (see Fig. 7 and Fig. 9). This is due to the fact that in case of inter-turn SC in two phases, the voltages of the SC windings are null. Therefore, the SC current and the healthy current are completely opposite, and the phase angle between the SC current and the back-EMF is $\pi/2$. Nevertheless, in case of the inter-turn and inter-phase SC, since the voltages of SC windings are no longer null, this phase angle is different from $\pi/2$. As a result, the average braking torque generated by the inter-turn and inter-phases SC windings is lower while the braking torque ripple is higher than the inter-turn SC in two phases. However, the higher increase in average braking

torque has been compensated by the speed controller by increasing healthy currents. This is the reason why the difference of speed drop between both types of SC is not large. The comparison of simulated braking torque between the inter-turn SC in two phases and the inter-turn and inter-phase SC is shown in Fig. 14. One conclusion can now be drawn that lower average braking torque involves lower healthy current increase and higher braking torque ripple leads to higher speed ripple.



(a)



(b)

Fig. 13 Simulated and measured currents before and after inter-turn and inter-phase SC for $\alpha = \beta = 25\%$ and at 102 rad/s. (a) simulated currents, (b) measured currents.

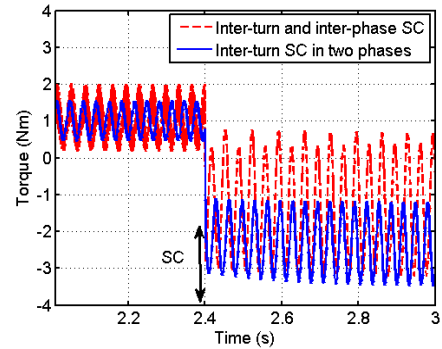


Fig. 14 Simulated braking torque generated by SC currents for the two cases: inter-turn and inter-phase SC and the inter-turn SC in two independent phases.

IV. CONCLUSION

In this paper, an analytical model is developed to investigate the inter-turn short-circuit (SC) fault in and between two phases in a 12-slot/10-pole flux switching

permanent magnet (FSPM) machine. The characteristics in terms of rotor speed, healthy and SC currents have been analysed. For both SC problems, it is found that at low rotor speeds, the value of α and β do not have a significant influence on the SC current. However, at high rotor speed, the lower α or β , the higher the SC current. The worst case is when only one turn is short-circuited.

Currents in healthy phases need to increase significantly to compensate the drop of electromagnetic torque due to the decrease in the number of healthy turns and the increase in braking torque produced by the SC currents. When $\alpha = 75\%$, an increase of five times in the healthy current is observed. In addition, over the entire investigated rotor speed range, the speed drops and the speed ripple increases with the increase in α or β .

In comparison with the inter-turn SC in two phases, with the same α or β , the speed drop of the inter-turn and inter-phase SC is similar while its speed ripple is much higher. The accuracy of the proposed simulation models have been extensively validated via experimental results on a prototype FSPM machine.

APPENDIX

Table 1 Parameters of the prototype 12-slot/10-pole FSPM machine

Stator slot number	12	Mutual inductance	2.18 mH
Rotor pole number	10	Self-inductance	4.6 mH
Stator outer radius	77.2 mm	Phase resistance	1.06 Ω
Rotor outer radius	43 mm	Iron material	Si-Fe 3%
Stack length	60 mm	Permanent magnet	SmCo
Air-gap length	0.2 mm	Remanence @200°C	0.8T
Slot fill factor	0.4	Rated power	1.12 kW
N° of turns per tooth	100	Rated speed	1000 rpm
Phase no-load flux-linkage	118 mWb	Rated RMS current	4.2 A

REFERENCES

- [1] J. T. Chen and Z. Q. Zhu, "Winding configurations and optimal stator and rotor pole combination of flux-switching pm brushless ac machines," *IEEE Trans. Energy Convers.*, vol. 25, no. 2, pp. 293-302, Jun. 2010.
- [2] Y. Shi, L. Jian, J. Wei, Z. Shao, W. Li, and C. C. Chan, "A new perspective on the operating principle of flux-switching permanent-magnet machines," *IEEE Trans. Ind. Electron.*, vol. 63, no. 3, pp. 1425-1437, Mar. 2016.
- [3] P. Taras, G. J. Li, and Z. Q. Zhu, "Comparative study of fault tolerant switched flux permanent magnet machines," *IEEE Trans. Ind. Electron.*, vol. 64, no. 3, pp. 1939-1948, Mar. 2017.
- [4] A. S. Thomas, Z. Q. Zhu, R. L. Owen, G. W. Jewell, and D. Howe, "Multiphase flux-switching permanent-magnet brushless machine for aerospace application," *IEEE Trans. Ind. Appl.*, vol. 45, no. 6, pp. 1971-1981, Nov.-dec. 2009.
- [5] Z. Q. Zhu, Y. Pang, D. Howe, S. Iwasaki, R. Deodhar, and A. Pride, "Analysis of electromagnetic performance of flux-switching permanent magnet machines by non-linear adaptive lumped parameter magnetic circuit model," *IEEE Trans. Mag.*, vol. 41, no. 11, pp. 4277-4287, Nov. 2005.
- [6] Z. Q. Zhu and D. Howe, "Electrical machines and drives for electric, hybrid, and fuel cell vehicles," *Proc. IEEE*, vol. 95, no. 4, pp. 746-765, Apr. 2007.
- [7] Z. Q. Zhu and J. T. Chen, "Advanced flux-switching permanent magnet brushless machines," *IEEE Trans. Mag.*, vol. 46, no. 6, pp. 1447-1453, Jun. 2010.
- [8] A. H. Bonnett and C. Yung, "Increased efficiency versus increased reliability," *IEEE Ind. Appl. Magazine*, vol. 14, no. 1, pp. 29-36, Jan.-Feb. 2008.
- [9] A. H. Bonnett and G. C. Soukup, "Cause and analysis of stator and rotor

failures in three-phase squirrel-cage induction motors," *IEEE Trans. Ind. Appl.*, vol. 28, no. 4, pp. 921-937, Jul./Aug. 1992.

- [10] A. Gandhi, T. Corrigan, and L. Parsa, "Recent advances in modeling and online detection of stator interturn faults in electrical motors," *IEEE Trans. Ind. Electron.*, vol. 58, no. 5, pp. 1564-1575, May 2011.
- [11] K.-C. Kim, S.-B. Lim, D.-H. Koo, and J. Lee, "The design of permanent magnet synchronous motor considering partial demagnetization on the permanent magnet," *IEEE Trans. Mag.*, vol. 42, no. 10, pp. 3485-3487, Oct. 2006.
- [12] M. Rosu, J. Saitz, and A. Arkkio, "Hysteresis model for finite-element analysis of permanent-magnet demagnetization in a large synchronous motor under a fault condition," *IEEE Trans. Mag.*, vol. 41, no. 6, pp. 2118-2123, Jun. 2005.
- [13] G. J. Li, X. Ojeda, E. Hoang, and M. Gabsi, "Thermal-electromagnetic analysis of a fault-tolerant dual star flux-switching permanent magnet motor for critical applications," *IET Elec. Power Appl.*, vol. 5, no. 6, pp. 503-513, Jul. 2011.
- [14] L. Romeral, J.C. Urresty, J.-R. Riba Ruiz, and A. Garcia Espinosa, "Modeling of surface-mounted permanent magnet synchronous motors with stator winding interturn faults," *IEEE Trans. Ind. Electron.*, vol. 58, no. 5, pp. 1576-1585, May 2011.
- [15] B. Vaseghi, B. Nahid-mobarakh, N. Takorabet, and F. Meibody-Tabar, "Inductance identification and study of pm motor with winding turn short circuit fault," *IEEE Trans. Mag.*, vol. 47, no. 5, pp. 978-981, May 2011.